Real-Time Implementation of Hybrid Visible Light/Infrared Communications Supporting Full-Range Dynamic Dimming Control

Shixin Liu, Xiaodi You, Jian Chen, *Member, IEEE*, Changyuan Yu, *Senior Member, IEEE*, Chaoran Xiong, Mingyi Gao, *Senior Member, IEEE*, and Gangxiang Shen, *Senior Member, IEEE*

***Abstract*—Implementing dimming control in visible light communication (VLC) systems often involves a trade-off that reduces data rates. To address this, we propose a hybrid visible light (VL)/Infrared (IR) communication scheme that leverages pulse amplitude modulation (PAM) symbols in both VL and IR spectra, alternating them within pulse width modulation (PWM) "ON" and "OFF" slots. By efficiently using PWM "OFF" slots, the achievable data rate drop due to dimming is mitigated without affecting illumination. To ensure synchronization during the switch between VL and IR links, we design real-time dimming control state machines at both ends of the link, enhancing link stability. Additionally, we develop an adaptive hybrid frame structure that dynamically adjusts the length of transmitted information as the duty cycle continuously changes, ensuring uninterrupted communication. Experimental results from implementation using field-programmable gate arrays (FPGA) demonstrate real-time transmission under precise full-range dimming control, dynamically ranging from 1 to 0 with a resolution of 0.0053, maintaining a consistent 10 Mb/s data rate at bit error rates (BERs) lower than 3.4×10^{-4} and 20 Mb/s at BERs lower than 7.0×10^{-3} within a link range of 0.53 m without light concentration at the transmitter. Compared to baseline VLC, our system achieves a 100% data rate improvement at a duty cycle of 0.5, and supports stable data transmission even in low-light conditions.**

***Index Terms*—Visible light communication (VLC), infrared (IR) communication, dimming control, pulse width modulation (PWM), field-programmable gate arrays (FPGA).**

Manuscript received 10 January 2024; accepted 10 January 2024. Date of publication 15 January 2024; date of current version 26 January 2024. This work was supported in part by the National Natural Science Foundation of China under Grant 62001319, in part by Suzhou Science and Technology Bureau-Technical Innovation Project in Key Industries under Grant SYG202112, in part by the Open Fund of IPOC (BUPT) under Grant IPOC2020A009, and in part by HK RGC GRF under Grant 15212720. *(Corresponding author: Xiaodi You.)*

Shixin Liu, Xiaodi You, Chaoran Xiong, Mingyi Gao, and Gangxiang Shen are with the School of Electronic and Information Engineering, Soochow University, Suzhou 215006, China (e-mail: 20224228043@stu.suda.edu.cn; xdyou@suda.edu.cn; crxiongfrank@stu.suda.edu.cn; mygao@suda.edu.cn; shengx@suda.edu.cn).

Jian Chen is with the School of Telecommunications and Information Engineering, Nanjing University of Posts and Telecommunications, Nanjing 210003, China (e-mail: chenjian@njupt.edu.cn).

Changyuan Yu is with Photonics Research Institute, Department of Electrical and Electronic Engineering, The Hong Kong Polytechnic University, Kowloon 999077, Hong Kong (e-mail: changyuan.yu@polyu.edu.hk).

Digital Object Identifier 10.1109/JPHOT.2024.3353776

I. Introduction

THE evolution of solid-state lighting has positioned visible light communication (VLC) as a complementary alternative wireless solution. VLC utilizes light-emitting diodes (LEDs) or laser diodes (LDs) for both illumination and data transmission, offering benefits such as spectrum license exemption, data security, and immunity to electromagnetic interference [1], [2]. Given the importance of illumination, dimming control is a critical function in VLC. Dimming control allows users to customize lighting according to their preferences, promoting energy conservation, reducing heat generation, and extending device lifespan, in line with eco-friendly principles [3], [4], [5]. However, integrating dimming control into VLC systems presents challenges, as it can potentially impact communication performance by reducing achievable data rates during dimming. Balancing this trade-off is crucial when designing VLC systems [6], [7], [8].

In recent years, extensive research has been dedicated to VLC dimming control, primarily focusing on techniques such as amplitude modulation (AM) and pulse width modulation (PWM) [9], [10], [11]. In AM-based approaches, brightness control relies on adjusting the current supplied to the light source, but this method may compromise dimming precision, reduce device lifespan, and cause chromaticity shift problems [12], [13]. In contrast, PWM-based approaches maintain a fixed current while varying the duty cycle of signal pulses, making them more commonly used for dimming control [14]. These schemes mainly prioritize efficient data transmission, especially when reducing the duty cycle, and they often employ high-efficiency modulation formats [15], [16], [17], [18], [19]. For example, discrete multi-tone was combined with PWM in [15], but this method imposes a limit on the system data rate. In pursuit of enhanced spectral efficiency (SE), we proposed integrating variable M-ary quadrature amplitude modulation (M-QAM) orthogonal frequency division multiplexing (OFDM) with PWM [16] and multi-pulse position modulation (MPPM) [17] for dimming control, respectively. However, the required M-QAM symbol rate still has a strong correlation with the duty cycle. At low dimming levels, maintaining constant rate transmission and reliable link quality necessitates significantly increased symbol rates and launching power. In [18], a reverse polarity optical OFDM method was introduced to utilize both the "ON" and "OFF"

TABLE I
COMPARISON OF DIMMING CONTROL EXPERIMENTS

Reference	Experiment	Platform	Dimming Range	Data Rate	Transmitter and Receiver	Distance	Dynamic Dimming
[20]	Offline	LabView	0.3, 0.7	10 Kb/s	1 LED, 1 PD	0.2 m	No
[21]	Offline	MATLAB	0.1 ~ 1	2.55 Kb/s	1 LED, 1 lens, 1 camera	0.2 m	No
[22]	Real-time	FPGA	0.4665 ~ 0.5184	N/A	1 LED, 2 lenses, 1 PD	3.6 m	No
[23]	Real-time	BBB	0.1 ~ 0.9	110 Kb/s	1 LED (4.7 W*), 1 PD	3.6 m	Yes
[24]	Real-time	ZedBoard	0.1 ~ 0.9	50 Kb/s	3 LEDs (10 W*), 1 PD	0.9 m	No
[25]	Real-time	Raspberry Pi	0.25, 0.5, 0.75	130 Kb/s	1 LED (2.4 W*), 1 PD	3.5 m	No
[26]	Real-time	ATmega128	0.05 ~ 0.95	40 Kb/s	9 LEDs, 1 lens, 1 PD	3 m	No
This work	Real-time	FPGA	0 ~ 1	20 Mb/s	1 VL LD (~80 mW#), 1 IR LD (~50 mW#), 1 lens, 1 PD	0.53 m	Yes

* means electrical power, # means optical power.

slots of PWM for data transmission, thus enhancing transmission efficiency. However, this approach constrains brightness levels within a specific range (e.g., 0.07 to 0.93) and affects dimming precision unless the duty cycle is precisely 0.5. We also proposed a hybrid visible light (VL)/infrared (IR) dimming control scheme based on MPPM, leveraging MPPM "ON" and "OFF" slots to transmit OFDM signals for accurate dimming across the entire dimming range [19]. However, achieving synchronization between OFDM and MPPM presents challenges, and latency remains a concern. It is important to note that all these studies have primarily been theoretical and simulation-based, lacking experimental validation.

To address this limitation, some studies conducted offline experiments to validate dimming control schemes [20], [21]. For example, in [20], on-off-keying (OOK) signals at 10 Kb/s were embedded into both the "ON" and "OFF" slots of PWM dimming control pulses. However, this method requires the transition time of PWM to coincide with that of OOK pulses. Consequently, it only demonstrated dimming control cases at 0.3 and 0.7, and its dimming accuracy was compromised [4]. To assess the practicality and real-world performance of dimming control schemes, some studies have conducted real-time experiments [22], [23], [24], [25], [26]. Table I compares various dimming control experiments. From Table I, it is evident that existing real-time dimming control systems face challenges, including low data rates and restricted dimming ranges. Moreover, they do not support dynamic dimming, which allows dimming levels to change without interrupting communication. Future dimming control demands precision and flexibility. To effectively integrate such dimming control into high-speed and real-time VLC systems, addressing these challenges is essential for enhancing the practicality of VLC.

In this paper, we propose a hybrid VL/IR communication scheme for dimming control based on PWM, which enables the cooperative use of both VL and IR links. To maximize data transmission efficiency, we strategically allocate specific pulse amplitude modulation (PAM) symbols in both VL and IR links by alternating them within PWM "ON" and "OFF" slots, thereby efficiently utilizing available time slot resources. Crucially, IR signals are imperceptible to the human eye, ensuring that incorporating an IR link does not affect the perceived brightness of VL. This facilitates stable data transmission while enabling precise dimming control and flexible adjustments to illumination levels, even when the VL source is turned off. The original concept of the proposed hybrid scheme was first introduced in our conference paper in a theoretical, early-stage context [27]. This work extends the concept and aims to realize it through real-time implementation. However, switching between VL and IR links introduces inherent timing challenges, driven by the user-determined, real-time slot durations for dimming and differences in modulation formats between the two links. These factors lead to dynamic changes in loaded data, leading to timing disparities and real-time processing complexities between both links. To tackle this issue, we design real-time dimming control state machines at both the transmitter and receiver. These state machines effectively resolve timing issues during transitions between VL and IR links. To support the implementation of these state machines, we further develop an adaptive hybrid frame structure capable of dynamically adjusting the length of transmitted information in response to real-time changes in the duty cycle. This design ensures that the system can load as much data as possible without interrupting communication, while also preventing the reception of erroneous information due to changes in the duty cycle. Importantly, no prior information regarding dimming levels needs to be transmitted. To validate the proposed scheme, we conduct experiments using FPGA and comprehensively evaluate critical parameters, including data rate, bit error rate (BER), bias voltage, and transmission distance at various dimming levels. Experimental results demonstrate that when employing precise full-range dimming control, dynamically from 1 to 0 with a resolution of 0.0053, the system achieves real-time transmission, maintaining a consistent data rate of 10 Mb/s at BERs lower than 3.4×10^{-4} and 20 Mb/s at BERs lower than 7.0×10^{-3} within a link range of 53 cm without light concentration at the transmitter. Notably, based on Table I, our scheme stands out as the only one capable of maintaining a steady data rate of up to 20 Mb/s under full-range dynamic dimming control.

The rest of this paper is organized as follow. Section II analyzes the proposed hybrid VL/IR communication scheme for dimming control. It also introduces the real-time dimming control state machines and the adaptive hybrid frame structure. Section III conducts experiments and evaluates the performance of the proposed scheme. We conclude the paper in Section IV.

II. Hybrid VL/IR Communication Scheme for Dimming Control

A. Working Principle

In conventional PWM-based dimming control schemes, achieving accurate dimming requires activating the VL link only during PWM "ON" slots for data transmission, leaving no data transmission during PWM "OFF" slots. Consequently, in this scheme, maintaining a constant data rate and reliable data transmission quality necessitates a significant increase in the required symbol rate and launching power as the duty cycle decreases, particularly at low dimming levels. Moreover, when the duty cycle reaches 0, as in total darkness, the conventional scheme becomes incapable of supporting data transmission. To address the issue of data transmission gaps during PWM "OFF" slots, we propose a hybrid VL/IR communication scheme in this paper. In this scheme, both VL and IR links transmit data alternately within PWM "ON" and "OFF" slots. This approach leverages an additional invisible IR link during PWM "OFF" slots to compensate effectively for the achievable data rate drop in the VL link due to dimming. This compensation ensures stable data rate transmission across the entire dimming control range. It is worth noting that there are two alternative approaches for compensation. The first approach involves using entirely independent VL and IR sources, where IR handles data transmission and VL manages lighting with dimming control. However, in this method, the rising and falling edges of the VL dimming control pulses can introduce interference to the IR link, thereby impacting the quality of IR transmission. In the second approach, in addition to IR transmission during PWM "OFF" slots, it involves activating the IR link during PWM "ON" slots to transmit the same data information as the VL link. Nevertheless, this approach requires precise synchronization between both links to avoid inter-symbol interference. Moreover, although activating the IR link in PWM "ON" slots can enhance the received signal-to-noise ratio (SNR) during these slots, it does not significantly improve the system's BER. Instead, it raises costs due to the additional IR energy consumption during PWM "ON" slots. Consequently, in our scheme, we adopt the method of alternating VL and IR data transmission within PWM "ON" and "OFF" slots.

It is important to note that the modulation bandwidth of IR sources typically surpasses that of VL sources due to the extensive history of IR communication and its applications in optical fiber communication. VL sources are primarily designed for illuminative purposes, with bandwidth being less of a priority. Consequently, in a hybrid VL/IR communication system, IR sources often serve to compensate for data loss in the VL link. However, in certain situations, if the IR link lacks sufficient bandwidth, it may be incapable of meeting the required data rate using the same modulation format as the VL link. To address this, higher modulation levels are applied to boost the data rate in the IR link. Currently, photo-detectors (PDs) used in VLC usually exhibit higher responsivity in the IR wavelength compared to VL responsivity, thanks to the well-established development of the IR industry. This suggests the feasibility of implementing high modulation formats in the IR link. When both bandwidth and modulation levels are constrained in the IR link, it can adversely affect data rates, particularly at low dimming levels or in darkness. In such cases, the IR link should be utilized to establish the fundamental data link. Prioritizing data services with higher importance is crucial, and services with lower priority may need to be deferred until higher dimming levels are restored.

Fig. 1 illustrates the schematic diagram of our proposed scheme, featuring a transmitter comprising a VL source and an IR source functioning as antennas. A PD, positioned on the receiver, is employed to detect the combined VL and IR signals. PAM is selected for data transmission due to its efficiency and ease of implementation using FPGA. At the transmitter, a PWM waveform is generated in accordance with the user's dimming control preferences. This PWM waveform plays a crucial role in determining the system operational state and signaling when data should be transmitted in both the VL and IR links. After amplitude adjustment, it can be represented by:

$$s_{PWM,VL}(t) = A_{VL} \sum_{k=0}^{+\infty} \begin{Bmatrix} \varepsilon\left(t - kn_tT_B\right) \\ -\varepsilon\left[t - \left(n_d + kn_t\right)T_B\right] \end{Bmatrix}, \quad (1)$$

where T_B is the PAM symbol duration, n_d is the number of PAM symbols transmitted in each PWM "ON" slot, n_t is the total number of PAM symbols within each PWM period, k is the index of PWM pulses, A_{VL} is the amplitude of the PWM waveform, and $\varepsilon(t)$ stands for the unit step function. Additionally, through an inverter, an inverted PWM waveform is generated to control the state of the IR source. After amplitude adjustment, it can be represented by:

$$s_{PWM,IR}(t) = A_{IR} \sum_{k=0}^{+\infty} \begin{Bmatrix} \varepsilon\left[t - \left(n_d + kn_t\right)T_B\right] \\ -\varepsilon\left[t - \left(k+1\right)n_tT_B\right] \end{Bmatrix}, \quad (2)$$

where A_{IR} is the amplitude of the inverted PWM waveform. Consequently, the PWM duty cycle for dimming control can be described as:

$$D = n_d/n_t. \quad (3)$$

Simultaneously, the transmitter processes the original data information into PAM pulse streams. This process begins by dividing the bipolar data stream from the data source into two separate streams based on the "ON" and "OFF" states of PWM. One stream is directed to the VL link, and the other is directed to the IR link. To maintain synchronization between transmission and reception, both streams are packaged and framed. Subsequently, they are mapped into PAM waveforms according to the modulation levels utilized by each link. After this mapping, the amplitude of the lth PAM symbol in the time domain for hybrid transmission is expressed by:

$$\begin{aligned} W_{VL/IR}(l) = & \sum_{i=(l-1)\log_2 M_{VL/IR}+1}^{l\log_2 M_{VL/IR}} V_{VL/IR} \\ & \times b_i \times 2^{l\log_2 M_{VL/IR}-i} \\ & - \left(M_{VL/IR} - 1\right) V_{VL/IR}/2, \end{aligned} \quad (4)$$

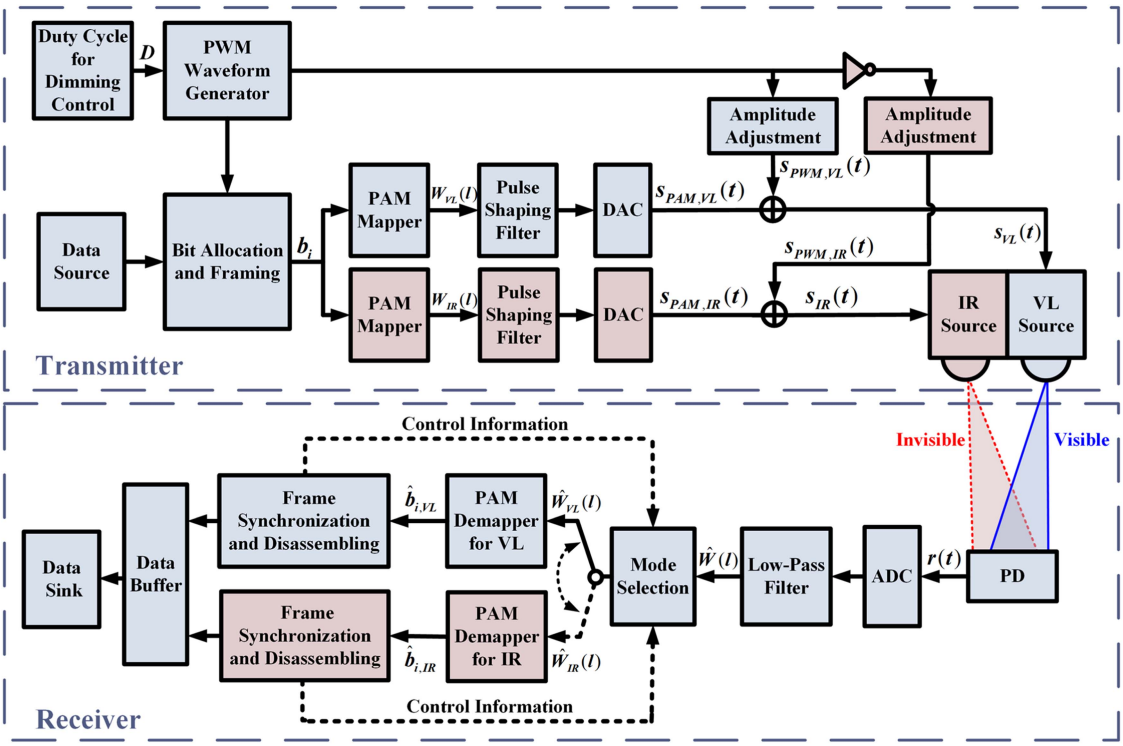

Fig. 1. Schematic diagram of the proposed hybrid VL/IR communication scheme.

where $V_{VL/IR}$ is the increment of PAM amplitude, $M_{VL/IR}$ is the PAM modulation level, and b_i is the value of the ith bit (i.e., 0 or 1) in the original data stream. In this paper, the subscript of VL/IR are used to distinguish the physical parameters for the VL and IR links, respectively. Following pulse shaping, the PAM pulse streams in the VL and IR links can respectively be described as:

$$s_{PAM,VL}(t) = \sum_{j=kn_t+1}^{kn_t+n_d} W_{VL}(j) g_{T_B}\left[t - \left(j - \frac{1}{2}\right) T_B\right], \tag{5}$$

$$s_{PAM,IR}(t) = \sum_{j=kn_t+n_d+1}^{(k+1)n_t} W_{IR}(j) g_{T_B}\left[t - \left(j - \frac{1}{2}\right) T_B\right], \tag{6}$$

where g_{TB} (t) is the pulse shaping function. After passing through digital-to-analog converters (DACs), the PAM pulse stream in the VL link is combined with the PWM waveform to modulate the VL source. Similarly, the PAM pulse stream in the IR link is combined with the inverted PWM waveform to modulate the IR source. The combined hybrid VL/IR signal can now be expressed as:

$$s_{VL/IR}(t) = s_{PAM,VL/IR}(t) + s_{PWM,VL/IR}(t). \tag{7}$$

Subsequently, this hybrid signal is alternately transmitted into the optical wireless channel, and its data rate is expressed as:

$$R_{hybrid} = \frac{D\log_2 M_{VL} + (1-D)\log_2 M_{IR}}{T_B}. \tag{8}$$

Fig. 2 illustrates an example of the combining process of the hybrid VL/IR signal waveform. In this example, we use OOK (2-level PAM) in both VL and IR links, with the original data stream being 0101011010111001 and the duty cycle of 0.625. As observed, the dimming level is determined by the VL signal waveform, which depends on both the duty cycle and the amplitude of the PWM waveform. As a means of conserving energy for the IR link, one viable strategy is to reduce the amplitude of the inverted PWM waveform.

In the hybrid VL/IR system, the channel gains of both VL and IR channels consist of the line-of-sight (LOS) and non-line-of-sight (NLOS) parts. The channel impulse response (CIR) between the light sources and the receiver can be modeled as [28], [29], [30]:

$$\begin{aligned} h_{VL/IR}(t) &= h_{VL/IR,LOS}(t) + h_{VL/IR,NLOS}(t) \\ &\approx H_{VL/IR}(0)\delta\left(t - \tau_{VL/IR,LOS}\right), \end{aligned} \tag{9}$$

where $h_{VL/IR,LOS}(t)$ is the CIR of the LOS part, $h_{VL/IR,NLOS}(t)$ is the CIR of the NLOS part, $\delta(\cdot)$ is the Dirac function, $\tau_{VL/IR,LOS}$ is the signal time delay of the LOS component, and $H_{VL/IR}(0)$ is the DC gain of the LOS channel. Because the LOS channel contains most of the transmitted power, this work focuses on a point-to-point link. We assume that the optical wireless channel only has the LOS part and ignore the NLOS part [6], [11], [29].

At the receiver, the hybrid VL/IR signal is detected by a PD, and the electrical signal at the output of the PD can be written by:

$$r(t) = \gamma_{VL} s_{VL}(t) * h_{VL}(t) + \gamma_{IR} s_{IR}(t) * h_{IR}(t) + w(t), \tag{10}$$

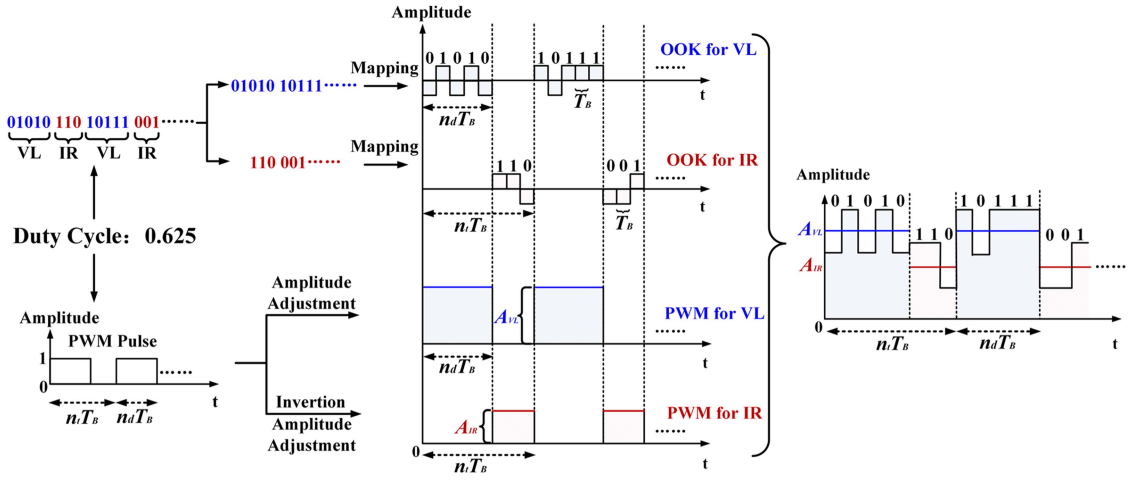

Fig. 2. Example of the combining process of the hybrid VL/IR signal waveform. ($D = 0.625$).

where $\gamma_{VL/IR}$ is the responsivity of the PD, $w(t)$ is the noise, and $*$ denotes convolution. The electrical signal is subsequently fed into an analog-to-digital converter (ADC) for conversion into a digital signal. Following this, it proceeds through filtering via a digital low-pass filter for signal demodulation. To demodulate the alternating VL and IR signals, different receiving modes are required. The determination of the receiving mode for the current data frame depends on various factors, including the receiving mode employed for the previous frame, the control information extracted from the previous frame, and the PAM modulation levels utilized. Once the mode is determined, the sampled signal is demapped. For example, for the lth OOK symbol, the demapping process can be described as:

$$\hat{b}_{i,VL/IR} = \begin{cases} 0, & \hat{W}_{VL/IR}(l) \\ & \leq \frac{1}{p_{VL/IR}} \sum_{j=1}^{p_{VL/IR}} \hat{W}_{VL/IR}(l-j) \\ 1, & \hat{W}_{VL/IR}(l) \\ & > \frac{1}{p_{VL/IR}} \sum_{j=1}^{p_{VL/IR}} \hat{W}_{VL/IR}(l-j) \end{cases}, \tag{11}$$

where $p_{VL/IR}$ is the number of bits transmitted in a preamble code (Please refer to Fig. 5). For the lth PAM4 symbol, the demapping process can be described as:

$$\hat{b}_{i+1,VL/IR}\hat{b}_{i,VL/IR} = \begin{cases} 00, & \hat{W}_{VL/IR}(l) \leq \frac{2\sum_{j=1}^{p_{VL/IR}/2} \hat{W}_{VL/IR}(l-j)}{3p_{VL/IR}} \\ 01, & \frac{2\sum_{j=1}^{p_{VL/IR}/2} \hat{W}_{VL/IR}(l-j)}{3p_{VL/IR}} \\ & < \hat{W}_{VL/IR}(l) \leq \frac{2\sum_{j=1}^{p_{VL/IR}/2} \hat{W}_{VL/IR}(l-j)}{p_{VL/IR}} \\ 10, & \frac{2\sum_{j=1}^{p_{VL/IR}/2} \hat{W}_{VL/IR}(l-j)}{p_{VL/IR}} \\ & < \hat{W}_{VL/IR}(l) \leq \frac{10\sum_{j=1}^{p_{VL/IR}/2} \hat{W}_{VL/IR}(l-j)}{3p_{VL/IR}} \\ 11, & \hat{W}_{VL/IR}(l) > \frac{10\sum_{j=1}^{p_{VL/IR}/2} \hat{W}_{VL/IR}(l-j)}{3p_{VL/IR}} \end{cases}. \tag{12}$$

The demapped bits are subsequently disassembled to extract the control information necessary for synchronization and link switchover. This information is then used to adjust the receiving mode for the subsequent frame. Finally, the recovered data is placed into the following data buffer and sent to the data sink in an organized manner, facilitating the reconstruction of the original data stream. Consequently, the BER for the original data stream is influenced by BER_{VL} and BER_{IR}, and this relationship is given by:

$$BER_{hybrid} = \frac{\begin{pmatrix} D\log_2 M_{VL} BER_{VL} \\ +(1-D)\log_2 M_{IR} BER_{IR} \end{pmatrix}}{D\log_2 M_{VL} + (1-D)\log_2 M_{IR}}. \tag{13}$$

B. Real-Time Dimming Control State Machines

In the real-time implementation of the hybrid VL/IR communication scheme, the system needs to switch between VL and IR time slots. These time slots can vary continuously due to user adjustments in lighting requirements. Additionally, there are differences in the modulation formats used for the VL and IR links. These factors introduce dynamic changes in the loaded data, resulting in timing disparities and complex real-time processing challenges during signal transmission and reception between both links. To ensure reliable data transmission despite timing disparities between the two links, rapid adaptation to the user's dimming requirements is crucial for both the transmitter and receiver. This adaptability becomes especially important when timing disparities exist between the two links, as it allows for the correct order of data transmission and ensures accurate demodulation of the hybrid signal. To meet these requirements and ensure that the system operates according to the correct timing logic while efficiently utilizing time slot resources for both links, we design real-time dimming control state machines for both the transmitter and receiver. These state machines are illustrated in Figs. 3 and 4, respectively. Correspondingly, we develop an adaptive hybrid frame structure that is compatible with the state machines, as illustrated in Fig. 5.

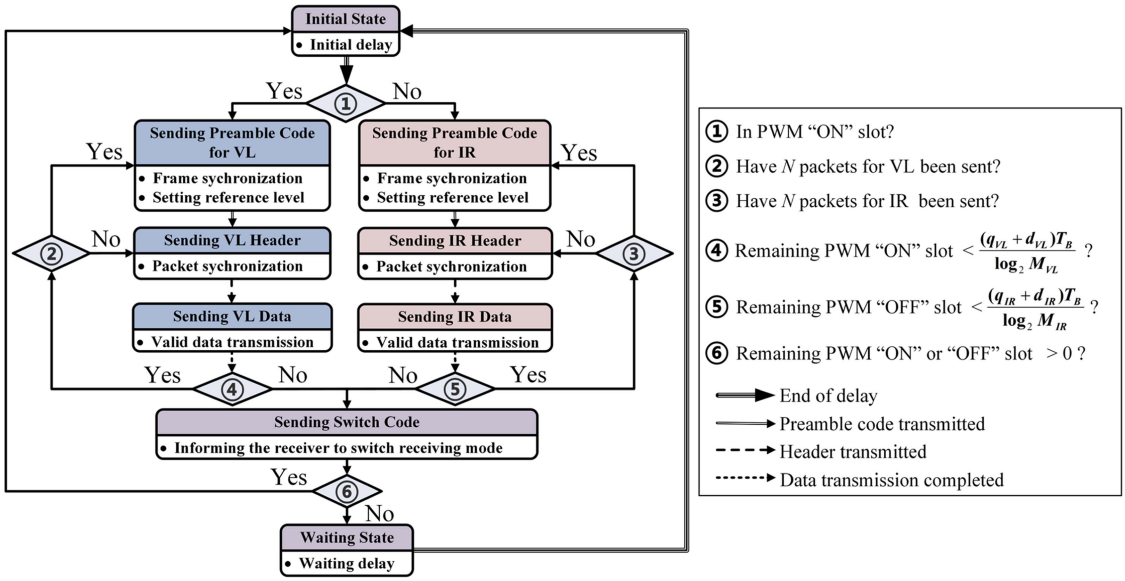

Fig. 3. Real-time dimming control state machine at the transmitter.

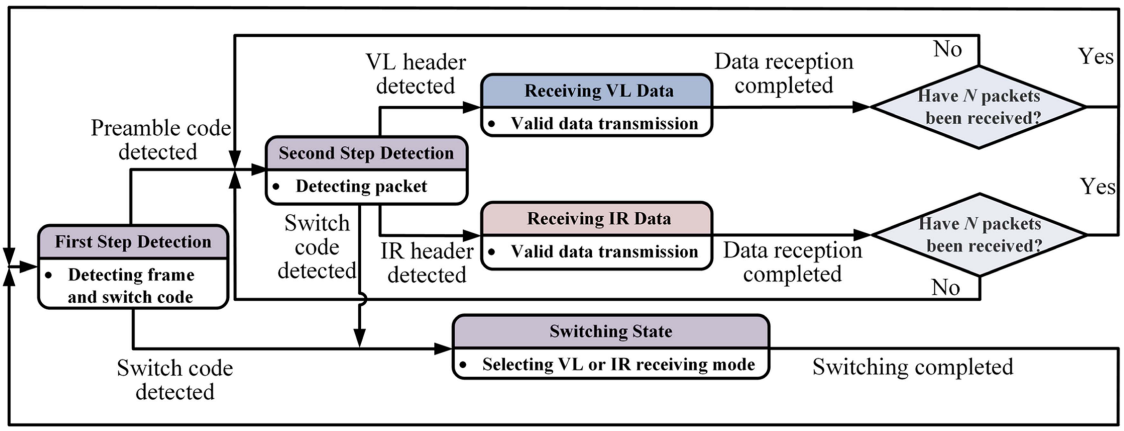

Fig. 4. Real-time dimming control state machine at the receiver.

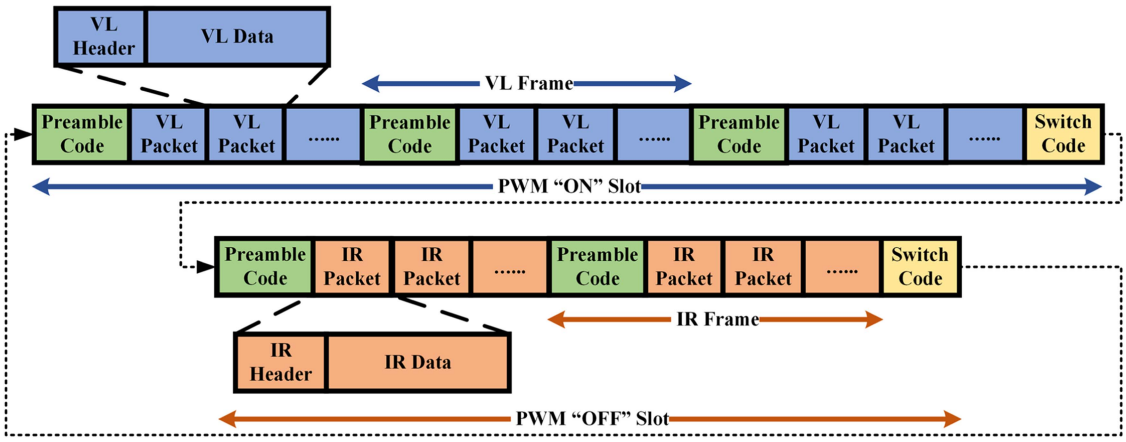

Fig. 5. Example of the adaptive hybrid frame structure. ($D = 0.6$).

In Fig. 3, the transmitter's state machine is primarily responsible for the accurate construction of frames from the alternating VL and IR links. It starts in the initial state at the beginning of each "ON" and "OFF" state, and following each time switch, to prepare the system and ensure its stability. The transmitter then determines whether to use the VL or IR link for communication based on the PWM "ON" and "OFF" states. Once the link is selected, the transmitter sends a preamble code for VL or IR to establish frame synchronization between the transmitter and receiver. The preamble code also aids the receiver in precomputing the decision threshold required for signal demodulation. Subsequently, the transmitter sends VL or IR headers for synchronizing data packets between the transmitter and receiver. It then proceeds to send VL or IR data. After completing data transmission, the transmitter calculates the remaining time within the PWM slot and determines whether it is sufficient to accommodate an entire packet. If there is enough time, the transmitter checks the count of packets transmitted within the current frame, denoted as N, representing the number of data packets within each frame. If N has not yet been reached, the transmitter proceeds to transmit another packet. However, once N is reached, the transmitter initiates a new frame. In situations where there is insufficient time, the transmitter sends a switch code to instruct the receiver to switch its receiving mode and then waits for the end of the slot. This cycle repeats continuously, enabling the alternate transmission of VL and IR signals.

In Fig. 4, the receiver's state machine primarily handles the tasks of signal detection, disassembly, and control of the receiving process. The detection process consists of two main steps. In the first step detection, the receiver identifies frames and the occurrence of a link switch. This is accomplished by detecting preamble codes and switch codes, respectively. When a preamble code is detected, it signifies the arrival of a frame. The preamble code is then used for frame synchronization and to update the decision threshold. Following this, the receiver enters the second step detection. In the second step detection, the receiver focuses on detecting packets and the occurrence of a link switch. This step involves the detection of VL or IR headers and switch codes. If VL or IR headers are detected, it indicates the arrival of a packet. Packet synchronization is then performed, and the VL or IR headers are further used to determine whether to receive VL data or IR data. Upon completing the reception of one data packet, the data is loaded into the data buffer and sent to the data sink in the correct order. This process continues until N packets from the VL or IR link are received. At this point, the receiver returns to the first step detection. Importantly, during both the first and second step detections, if a switch code is detected, the receiver switches the receiving mode for demodulation between VL and IR links and then returns to the first step detection. The inclusion of the switch code ensures that the receiver can correctly demodulate and demap the hybrid signals without prior information of the PWM duty cycle.

C. Adaptive Hybrid Frame Structure

To effectively implement the state machine and enable real-time dynamic dimming control, it is essential to dynamically adjust the length of the transmitted data frames to match the duration of PWM "ON" and "OFF" slots. Using a fixed-length frame structure would not be suitable as it cannot adapt to changes in the duty cycle. This inflexibility can lead to incomplete data frames being transmitted during dynamic dimming control, causing timing disparities in the state machine and disrupting the communication process. To overcome this issue, it is crucial to establish a relationship between the length of the data frame, the PWM duty cycle, and the duration of PWM "ON" and "OFF" slots. Based on this, we develop an adaptive hybrid frame structure as illustrated in Fig. 5. This frame structure automatically adjusts the number of frames according to the duration of PWM "ON" and "OFF" slots and adapts the number of data packets in the last frame transmitted in each time slot according to the remaining time. The advantage of this frame structure is that it can adapt to transmit as many data packets as possible under dynamically changing duty cycles, ensuring that the communication remains robust during dynamic dimming.

To ensure that our frame structure seamlessly aligns with the PWM waveform, it becomes imperative to fine-tune both the quantity of frames transmitted within each time slot and the composition of every individual frame. These adjustments must adhere to the following criteria:

$$\frac{L_{VL}p_{VL} + K_{VL}q_{VL} + K_{VL}d_{VL} + v}{\log_2 M_{VL}} = n_d, \tag{14}$$

$$\frac{L_{IR}p_{IR} + K_{IR}q_{IR} + K_{IR}d_{IR} + v}{\log_2 M_{IR}} = n_t - n_d, \tag{15}$$

where $L_{VL/IR}$ is the number of frames transmitted in each PWM "ON" or "OFF" slot, $K_{VL/IR}$ is the number of packets transmitted in each PWM "ON" or "OFF" slot, $q_{VL/IR}$ is the number of bits transmitted in a header, $d_{VL/IR}$ is the number of bits transmitted in the valid data of each packet, and v is the number of bits transmitted in a switch code.

After determining the frame structure, the theoretical resolution of the duty cycle, which represents the smallest increment of the duty cycle for dimming control, can be calculated as:

$$\Delta D = \mathrm{LCM}\left\{\frac{q_{VL} + d_{VL}}{n_t \log_2 M_{VL}}, \frac{q_{IR} + d_{IR}}{n_t \log_2 M_{IR}}\right\}, \tag{16}$$

where LCM denotes the calculation of the least common multiple. In this situation, the preamble code represents only a small portion of the entire PWM period. Therefore, we focus on assessing the influence of the header and data while disregarding the preamble code. Furthermore, since there is a need to switch between links, the transmission of a switch code becomes necessary. Consequently, apart from the duty cycles of $D_{\min} = 0$ and $D_{\max} = 1$, the minimum and maximum dimming levels supported by the system are also influenced, which can be theoretically expressed by:

$$D_{Hmin} = \frac{v}{n_t \log_2 M_{VL}}, \tag{17}$$

$$D_{Hmax} = 1 - \frac{v}{n_t \log_2 M_{IR}}. \tag{18}$$

Considering both the dimming control resolution and the impact of the switch code, the system's supported dimming control

range is ultimately defined as:

$$D \in \{x | x = D_{Hmin} + u \times \Delta D, u \in N\} \cap \{x | D_{Hmin} \leq x \leq D_{Hmax}\} \cup \{D_{\min}, D_{\max}\}. \quad (19)$$

It is worth mentioning that, in comparison with the scheme in [19], where MPPM is combined with OFDM, the combination of PWM and PAM is more suitable for real-time implementation due to its simplicity and effectiveness in three aspects: (1) System implementation complexity. Compared to the straightforward mapping in PWM, MPPM tends to be more intricate due to increased symbol variability, stringent coding requirements, and the necessity for sophisticated signal processing techniques at the receiver. Additionally, MPPM may exhibit greater sensitivity to errors. On the other hand, implementing OFDM in hardware can be more complex than implementing PAM due to the requirements for multiple subcarriers, fast Fourier transform (FFT)/inverse FFT (IFFT) operations, and synchronization mechanisms. Consequently, the combination of PWM and PAM is notably simpler to implement than the combination of MPPM and OFDM. (2) Synchronization and switching flexibility of the hybrid VL/IR signals. In the case of MPPM+OFDM, the long frame length of OFDM necessitates splitting the OFDM symbol into several parts during dimming control, each carried within the duration of an MPPM chip. Achieving synchronization between MPPM and OFDM demands sophisticated calculations of frame parameters to ensure accurate demodulation of both signals at the receiver. Additionally, more complex switching logic is required to facilitate smooth transitions between VL and IR receiving modes and ensure the correct demodulation of different pulse timing information at the receiver. On the contrary, PAM and PWM in the time domain can be achieved through simple clock synchronization, providing easier management in switching between VL and IR receiving modes. Each PAM symbol is transmitted within a PWM "ON" or "OFF" slot, making synchronization more straightforward. With a short switch code, no priori information about the dimming level is required. (3) Latency during dynamic dimming control. In scenarios involving dynamic dimming control, adopting both MPPM and OFDM entail long frames. If the MPPM frame is short, it may not support data efficiency, and if the MPPM or OFDM frame is long, the frame transmission must conclude before transitioning to a new dimming level, thereby introducing latency. In contrast, PWM carries independent PAM data packet, and the delay is confined within the length of a data packet, which is far shorter than a PWM period (Please refer to Fig. 5), making it well-suited for dynamic dimming applications.

III. Experiments and Discussions

A. Experimental Setup

In this section, we perform a series of experiments to assess the performance of the proposed hybrid VL/IR communication scheme designed for dimming control. Fig. 6(a) illustrates the real-time experimental setup used for our scheme. Since point-to-point scenarios represent the fundamental and widely adopted approach in current dimming control experiments, our experimental setup is based on point-to-point to validate the feasibility of our proposed scheme, at a distance suitable for scenarios such as VLC using a table lamp, within a vehicle, or aboard an aircraft. We use Spartan-6 FPGA development (DEV) boards (Alinx, AX545) at both ends to handle signal processing tasks, with the monitoring refresh frequency of state machines synchronized at 50 MHz. At the transmitter, the original bipolar data stream is stored in the read-only memory (ROM) intellectual property (IP) core of the DEV board. These data consist of a total of 460800 bits and are transmitted in a circular manner throughout the experiments. To control the dimming level, the PWM signal is generated by the DEV board, and its duty cycle is adjusted using the keyboard on the DEV board, allowing for variations from 1 to 0. When a request to modify the PWM duty cycle is received, the state machine dynamically adjusts the number of VL and IR frames to ensure uninterrupted communication during dimming control. Depending on the duty cycle, the state machine accesses the data and directs them to the first-in-first-out (FIFO) control, where they are divided into two branches. Subsequently, PAM waveforms are generated at a rate of 10 Msymbols/s in both branches. In our experiments, we adopt OOK and 4-level PAM (PAM4) due to their simplicity for implementation. After passing through a dual-channel DAC (Alinx, AN9767), the signals are combined with a PWM and an inverted PWM waveform, respectively, using a self-made dual-channel driver circuit. These signals are then modulated alternately onto two off-the-shelf LDs: the blue VL LD (OSRAM, PL450B, peak wavelength: ∼450 nm) and the IR LD (SHHO, SLD980050TN-A, peak wavelength: ∼980 nm). Finally, these modulated signals are emitted into the optical wireless channel for transmission. Note that both light beams diverge, and no light concentration is implemented at the transmitter to facilitate illumination across larger areas.

After passing through a plano-convex lens, the optical wireless signals are received by the PD (Thorlabs, PDA100A2), followed by a dual-channel ADC (Alinx, AN9238). Then, the sampled OOK or PAM4 signals enter the DEV board for digital low-pass filtering. They are then demodulated into a bipolar data stream based on the current state machine of VL/IR receiving mode. Following demodulation, the data stream is disassembled into different parts. The preamble codes, frame headers, and switching codes are utilized to refresh the state machine, and the data are sent to the upper computer through an Ethernet connection for BER calculation. Additionally, we use a digital storage oscilloscope (RIGOL, DS1102) to analyze and evaluate the received waveform after PD.

Fig. 6(b) displays the photographs of the experimental setup. In this figure, d_1 is the distance between the LDs and the lens, d_2 is the distance between the lens and the PD. Additionally, there are labeled points A, B, and C, serving as measurement positions for illuminance using a light meter (UNI-T, UT383). These points are located at approximately 10 cm, 53 cm, and 80 cm away from the LDs, respectively. On the DEV board, two keys are utilized to adjust the PWM duty cycle dynamically. One key increases the duty cycle, typically by 0.1, while the other key decreases it by the same amount. A self-made driving circuit is employed to divide the PWM waveform generated by the DEV

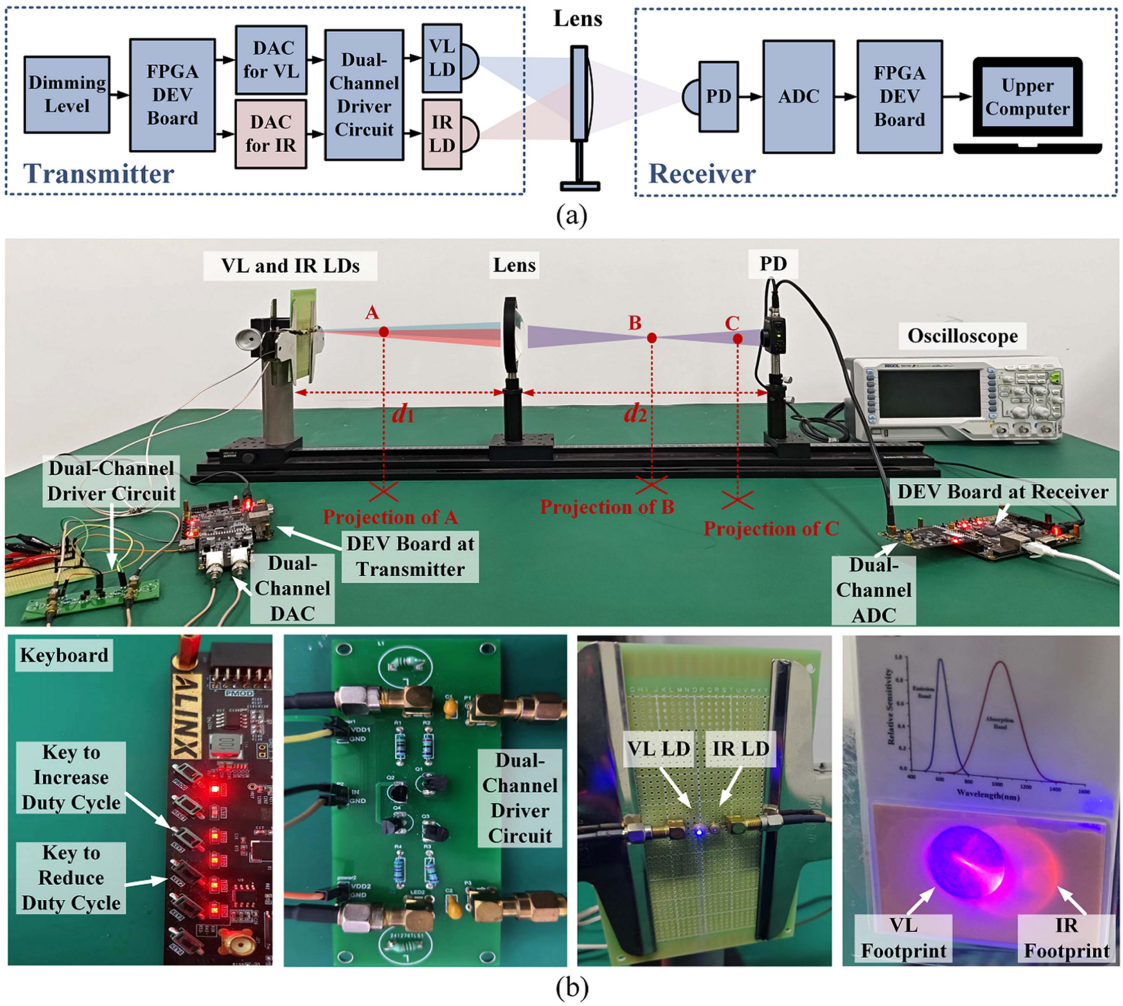

Fig. 6. (a) Real-time experimental setup for the proposed hybrid VL/IR communication scheme; and (b) photographs of the experimental setup.

board into two complementary PWM waveforms, then amplify them and combine them with PAM signals to modulate the VL and IR LDs, respectively. In our experiment, except for Fig. 10, the bias voltage of VL and IR LDs, corresponding to PWM "ON" and "OFF" slots, is set at 5.2V and 3.3V, respectively. The VL and IR LDs are placed close to each other to ensure stable transmission of hybrid signals. For capturing the optical footprint of the link at the receiver, a VL/IR detection card is used. Importantly, the position of the received optical footprint is symmetrical to that of the LDs, thanks to the lens conversion. Table II summarizes key experimental parameters of our system.

TABLE II
EXPERIMENTAL PARAMETERS

Parameter	Value
FPGA refresh frequency	50 MHz
PWM frequency	54.35 Hz
PAM symbol rate	10 Msymbols/s
Optical output power of VL LD	~80 mW
Optical output power of IR LD	~50 mW
Output wavelength of VL LD	450 nm
Output wavelength of IR LD	980 nm
Bias voltage of VL LD	5.2 V
Bias voltage of IR LD	3.3 V
PD Responsivity at 450 nm	0.24
PD Responsivity at 980 nm	0.72
PD aperture diameter	9.8 mm
Inner diameter of lens	100 mm
Focus length of lens	25 cm

B. Experimental Results and Discussions

We first evaluate the communication performance of our hybrid VL/IR communication scheme. Fig. 7 shows the waveform received after the PD, as observed by an oscilloscope, with a link range of 53 cm. In this figure, the PWM duty cycle is set at 0.6, and the PWM period is set at 0.0184 s, which means the frequency is higher than 50 Hz to alleviate the flickering effect. It is clear that the waveform is formed by a PWM and an inverted PWM waveform, each carrying different data frames, corresponding to (10). During PWM "ON" slots, VL frames carrying PAM4 symbols are received, while during PWM "OFF" slots, IR frames carrying OOK symbols are received. For more details, let us take PWM "ON" slots as an example. During each "ON" slot, we transmit five complete frames and one incomplete frame. The complete frames include a set of preamble codes

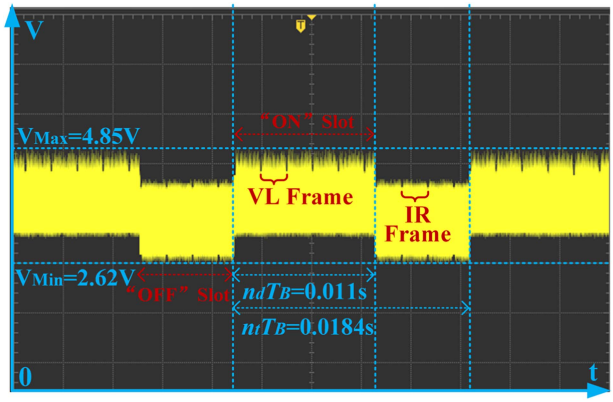

Fig. 7. Received waveform after the PD in our hybrid VL/IR communication scheme. ($d_1 = 30$ cm, $d_2 = 23$ cm).

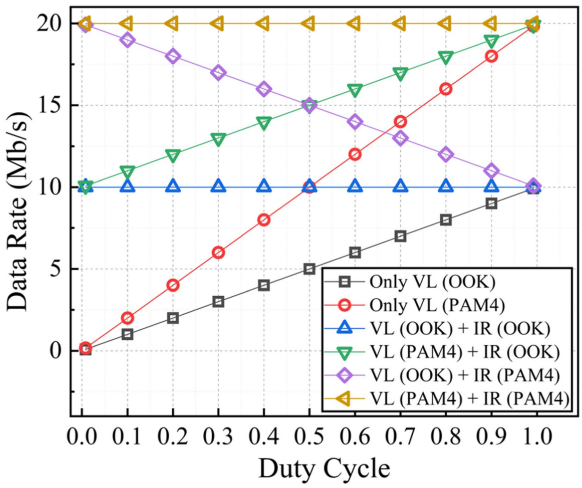

Fig. 8. Comparison of achievable real-time system data rates across various dimming levels. ($d_1 = 30$ cm, $d_2 = 23$ cm).

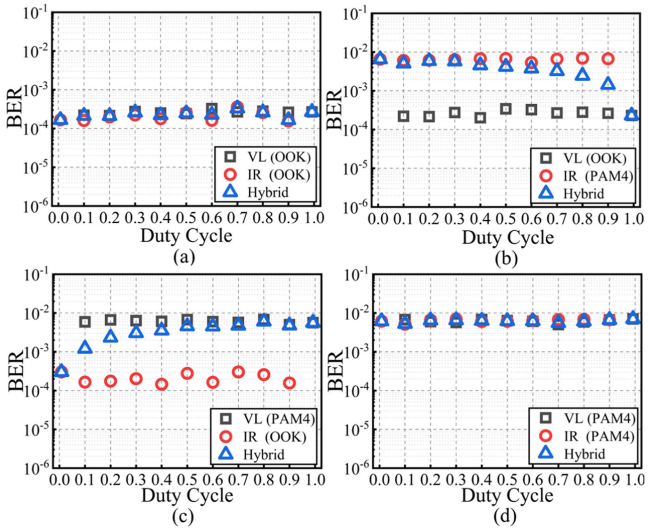

Fig. 9. Comparison of BERs in the hybrid VL/IR links corresponding to the curves in Fig. 8, with (a) OOK in both VL and IR; (b) OOK in VL and PAM4 in IR; (c) PAM4 in VL and OOK in IR; and (d) PAM4 in both VL and IR. ($d_1 = 30$ cm, $d_2 = 23$ cm).

transmitted before each frame for threshold determination and frame synchronization. The incomplete frame occurs when the system state machine flexibly adjusts the frame length, i.e., the number of packets, based on the remaining time of the "ON" slot. This adjustment allows us to transmit as much data as possible to enhance data transmission efficiency while ensuring precise dimming without interrupting communication. Similar conclusions can also be observed in PWM "OFF" slots.

To evaluate the link transmission quality, Fig. 8 compares the achievable real-time system data rates across various dimming levels with and without the utilization of the hybrid scheme, under a link range of 53 cm, where the most stable SNR is achieved beside the lens focus. In the conventional scheme where IR is not employed (considered as the baseline VLC), the maximum data rates of 10 Mb/s for OOK or 20 Mb/s for PAM4 are only attainable when dimming control is not in effect, i.e., the duty cycle is set to 1. However, when dimming control is applied, the achievable data rates are directly proportional to the PWM duty cycle. For instance, with a duty cycle of 0.5, the achievable data rates drop to 5 Mb/s and 10 Mb/s for OOK and PAM4, respectively, using only the VL link. Furthermore, in a dark scenario where the light is turned off, the achievable data rate becomes 0 Mb/s, rendering data transmission impossible. In contrast, our proposed hybrid VL/IR communication scheme enables stable data rates of 10 Mb/s for OOK or 20 Mb/s for PAM4 across the entire duty cycle range from 1 to 0, even in total darkness. Compared to the baseline VLC, the data rate improvement is 100% at a duty cycle of 0.5 and exceeds 100% at duty cycles less than 0.5. Thus, the IR link effectively compensates for the achievable data rate drop due to dimming. Moreover, by employing the IR link to carry modulation formats with higher SE, it becomes possible to enhance data capacity. For instance, at a duty cycle of 0.5, the achievable data rate with OOK in both VL and IR link is stable at 10 Mb/s. However, when PAM4 is utilized in the IR link, the data capacity is improved to 15 Mb/s at the same dimming level. Therefore, the hybrid scheme not only maintains data rates but also has the potential to increase them. It is worth noting that for VLC experiments targeting data rate records up to the Gb/s level, dedicated devices, including light sources and PDs with higher bandwidth, would be necessary. However, it is important to acknowledge that in our current experiment, the bandwidths of both the LD and PD are in the order of 10 Mb/s, with a symbol rate of 10 Msymbols/s. If experimental platforms with devices featuring higher bandwidth are employed, we believe our proposed scheme will remain effective and seamlessly integrate into these platforms.

Corresponding to the curves in Fig. 8, Fig. 9 compares the BERs in the hybrid VL/IR links under different dimming levels. The plotted BER curves include those for the VL link, IR link, and the hybrid BER of both links using (13). In Fig. 9(a), where both VL and IR links use OOK, the hybrid BERs consistently remain below 10^{-3} across the entire duty cycle range from 1 to 0. The highest hybrid BER is achieved at a duty cycle of 0.7, with a value of 3.4×10^{-4}. Similarly, in Fig. 9(d), when both VL

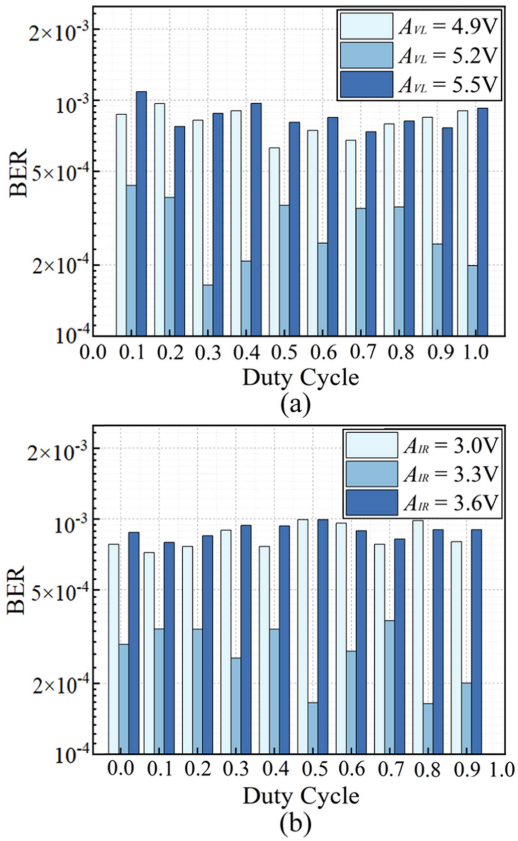

Fig. 10. Comparison of BERs for (a) the VL link; and (b) the IR link, with varying bias voltage applied to the LDs. ($d_1 = 30$ cm, $d_2 = 23$ cm).

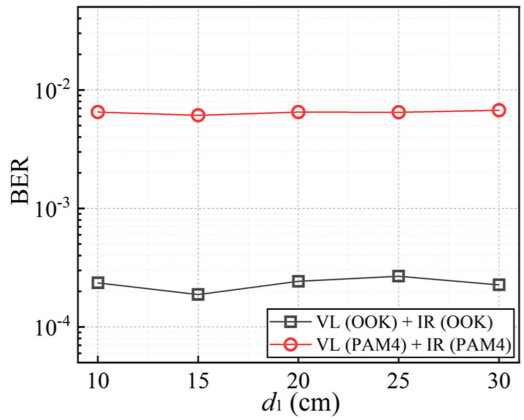

Fig. 11. Comparison of average BERs when varying the distance between the LDs and the lens. ($d_2 = 23$ cm).

and IR links use PAM4, the hybrid BERs remain below 10^{-2} for the entire duty cycle range from 1 to 0. The highest hybrid BER occurs at a duty cycle of 1, with a value of 7.0×10^{-3}. These BER levels indicate reliable system transmission quality, and further improvements can be achieved by implementing forward error correction (FEC) techniques [31], [32]. The individual BERs of VL and IR links are relatively insensitive to changes in the duty cycle. This is because the modulation format of each link remains constant during dimming, resulting in a consistent SNRs and BERs. However, the hybrid BER depends on the modulation formats used in both links and the duty cycle. For a fixed duty cycle, the hybrid BER lies between the BERs of the VL and IR links. For example, in Fig. 9(b), where the VL and IR transmission formats are OOK and PAM4, respectively, the individual BERs are approximately in the order of 10^{-4} and 10^{-3}. The hybrid BERs fall within this range and are distributed between the two. When the duty cycle varies, a larger duty cycle aligns the hybrid BER closer to the VL link performance, whereas a smaller duty cycle aligns it closer to the IR link performance, as evident in Fig. 9(b) and (c).

In Fig. 10, a bar graph is utilized to compare the BERs for both the VL and IR links across different dimming levels, while applying varying bias voltages to the LDs. OOK is used in both links. Specifically, for the VL LD, bias voltages of 4.9V, 5.2V, and 5.5V are applied, while for the IR LD, bias voltages of 3.0V, 3.3V, and 3.6V are applied. It is evident that the bias voltage has a significant impact on the BER performance of both links across all duty cycles. This influence arises from two factors. Firstly, when the bias voltage is low, it results in a weak signal, causing the LDs to operate abnormally and leading to poor SNRs received by the PD. Conversely, when the bias voltage is increased and generates excessive heat, the efficiency of LDs is diminished, thereby negatively impacts the demodulation performance at the receiver. As a result, in our experiments, the optimal bias voltages of 5.2V and 3.3V are selected for the VL and IR LDs, respectively. Additionally, it is noteworthy that despite the IR LD having a much lower bias voltage than the VL LD, their BERs are similar, as shown in both Figs. 9 and 10. This similarity arises from the higher responsivity of the PD in the IR wavelength compared to the VL. Consequently, the use of a low-power IR link indicates energy conservation when compared to using only a VL link.

To evaluate the robustness of our scheme against variations in terminal positions, Fig. 11 compares the average BERs measured when varying the distance d_1 between the LDs and the lens while keeping the distance d_2 between the lens and the PD fixed at 23 cm. These BER values represent the average performance under various dimming levels, ranging from 1 to 0. In Fig. 11, minimal changes in the hybrid BER are observed as d_1 is adjusted. When d_1 varies from 10 cm to 30 cm, the BER fluctuates between 1.9×10^{-4} and 2.7×10^{-4} when using OOK in both links, and between 6.1×10^{-3} and 6.7×10^{-3} when using PAM4 in both links, respectively. This stability is attributed to the consistent light emission from the LDs and the efficient focusing of the lens, resulting in negligible energy loss due to variations in d_1. Consequently, the received SNR remains unaffected.

In practical scenarios, misalignment of the communication link may occur. To assess the impact of non-ideal alignment, we examine three cases by experiments: vertical misalignment, horizontal misalignment, and rotational adjustment, depicted in Fig. 12(a), (b), and (c), respectively. The transmitter remains fixed, and d_1 is kept at 30 cm throughout the analysis. For vertical misalignment, the receiver either moves closer or farther away from the transmitter. For horizontal misalignment, it refers to a

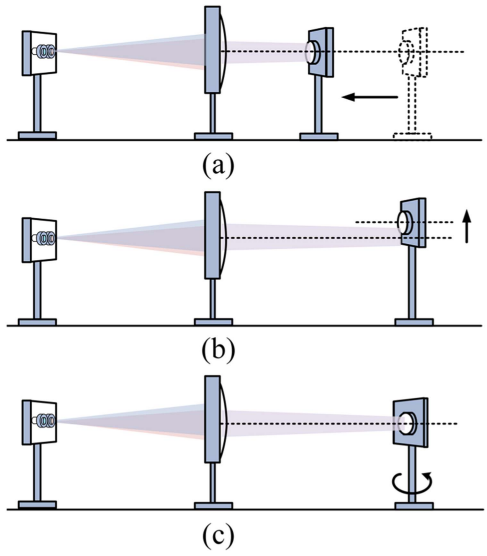

Fig. 12. Misalignment of communication link: (a) Vertical misalignment; (b) horizontal misalignment; and (c) rotational adjustment. ($d_1 = 30$ cm).

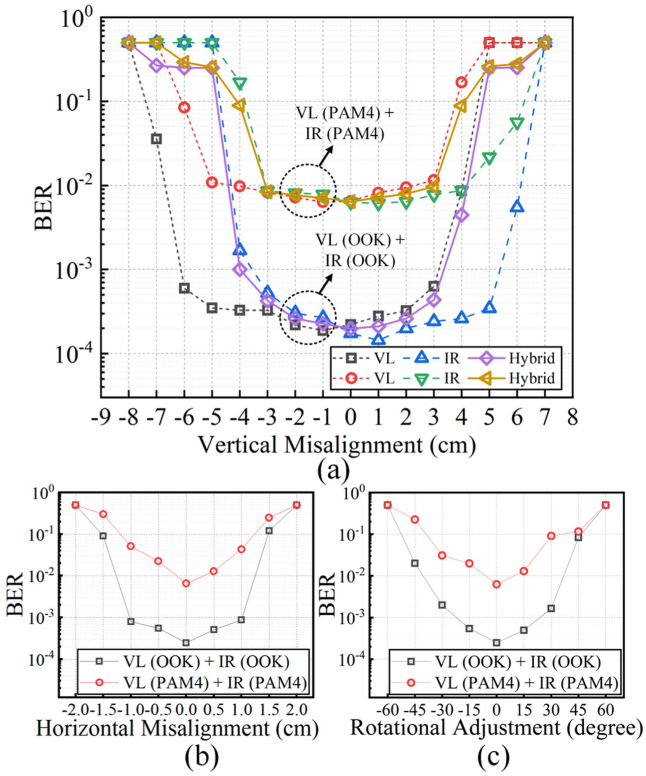

Fig. 13. Comparison of average BERs during: (a) Vertical misalignment; (b) horizontal misalignment; and (c) rotational adjustment. ($d_1 = 30$ cm).

situation where the optical axis of the receiver does not align with that of the transmitter. For rotational adjustment, the receiver rotates around the support rod.

Fig. 13(a), (b) and (c) compares the average BERs during vertical misalignment, horizontal misalignment, and rotational adjustment, respectively. In Fig. 13(a), significant variations in the hybrid BER are evident during vertical misalignment, where a negative value represents the receiver moving closer to the transmitter. For instance, when the vertical misalignment is -1 cm, -3 cm, and -5 cm, the BER values are measured at 2.3×10^{-4}, 4.3×10^{-4}, and 0.25, respectively, when using OOK in both links. Similar results are observed when using PAM4 in both links. This variation is attributed to changes in the distance between the PD and the lens focus. When the receiver moves out of the lens focus, the optical footprint received by the PD becomes larger than the effective area of the PD, resulting in a decrease in the received SNR and an increase in the BER. Additionally, it is noteworthy that the optimal BER ranges for the VL and IR links overlap, but not entirely. This discrepancy arises from the relative positions of the LDs and potential errors in the welding direction, causing an offset in the optical footprints of VL and IR, as confirmed by Fig. 6(b). Improving the welding process can lead to a larger overlapping range for better BER performance. In Fig. 13(b), significant variations in the hybrid BER are also evident during horizontal misalignment, where a negative value represents the optical axis of the receiver is lower than that of the transmitter. When adopting OOK in both links, a BER less than 10^{-3} is achieved for horizontal misalignment within 1 cm. However, when the horizontal misalignment exceeds 1 cm, BER degrades due to the failure to receive the optical footprint. Similar trends are observed when using PAM4 in both links. Specifically, at horizontal misalignment of -1 cm, BER is 5.1×10^{-2}. In Fig. 13(c), the hybrid BER increases with the growing rotational adjustment, where a negative value represents the receiver rotating around the support rod clockwise from a bird's-eye view. When using OOK in both links, the BER is 5.4×10^{-4} and 2.0×10^{-3} at rotational angles of $-15°$ and $-30°$, indicating reliable transmission for rotational adjustments less than 30°. For PAM4, the rotational tolerance becomes lower for maintaining reliable transmission quality.

Next, we assess the illumination performance of the proposed VL/IR communication scheme. To evaluate dimming control accuracy and limits, Table III presents the resolution and range of duty cycle supported by our system when different modulation formats are adopted in both links. The table includes both the tested results and the theoretical results calculated using (17), (18), and (19). D_L denotes the range that allows for completely linear dimming control. From Table III, it is evident that our system achieves a dimming control resolution of 0.0053, enabling high-precision dimming. The system supports a duty cycle range from 1 to 0, covering the entire dimming range. The completely linear dimming range D_L accounts for 99.55% of the total dimming range. However, there is a discrepancy between the theoretical and tested values. This variation is mainly due to certain module delays in our real-time FPGA setup, including the delay of the keyboard and DAC timing, which impacts the accuracy of the duty cycle resolution.

Fig. 14 displays the illuminance measurements taken at points A, B, and C, as labeled in Fig. 6(b), across various dimming levels. We consider the use of OOK and PAM4 in both links, respectively. Notably, the variation in illuminance at these three points exhibits a linear relationship with the PWM duty cycle. This observation emphasizes that our scheme not only enables stable data transmission but also fulfills the user's requirements

TABLE III
RESOLUTION AND RANGE OF THE DUTY CYCLE SUPPORTED BY OUR SYSTEM FOR DIMMING CONTROL

	ΔD		D_{min} / D_{max}	D_{Hmin}		D_L	D_{Hmax}	
	(17)	Tested	Tested	(18)	Tested	Tested	(19)	Tested
VL (OOK) + IR (OOK)	0.0012	0.0053	0 / 1	0.00007	0.0008	0.0022 ~ 0.9976	0.99993	0.9992
VL (OOK) + IR (PAM4)	0.0012	0.0053	0 / 1	0.00007	0.0008	0.0022 ~ 0.9988	0.99993	0.9995
VL (PAM4) + IR (OOK)	0.0012	0.0053	0 / 1	0.00004	0.0005	0.0012 ~ 0.9976	0.99996	0.9992
VL (PAM4) + IR (PAM4)	0.0006	0.0026	0 / 1	0.00004	0.0005	0.0012 ~ 0.9988	0.99996	0.9995

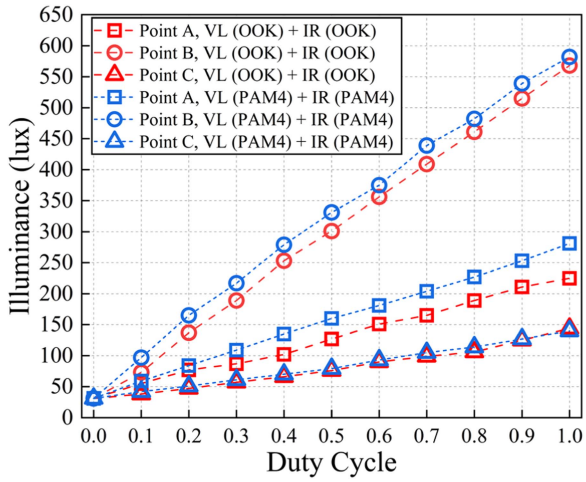

Fig. 14. Measured illuminance across various dimming levels at points A, B, and C.

by achieving a linear increase in illuminance for dimming control. Specifically, Point A, located before the lens and in close proximity to the LDs, exhibits moderate illuminance. In contrast, Point B has the highest illuminance as it is positioned closest to the lens focus, thus receiving the most energy. Point C, being farther away from the source, experiences light dispersion, resulting in dispersed energy. This trend aligns with the BER trends observed in Fig. 13(a).

IV. CONCLUSION

We proposed a hybrid VL/IR communication scheme for VLC dimming control, wherein VL and IR PAM signals are transmitted alternately within PWM "ON" and "OFF" slots. Real-time dimming control state machines were designed for both the transmitter and receiver, complemented by an adaptive hybrid frame structure. Experimental results showed the effectiveness of our scheme in compensating for data rate drops due to dimming, especially in low-light scenarios or when the light is turned off. With a resolution of 0.0053, employing an 80 mW VL LD and a 50 mW IR LD, our system achieved real-time transmission while dynamically changing the duty cycle from 1 to 0. Without light concentration at the transmitter, we achieved a consistent 10 Mb/s data rate at BERs lower than 3.4×10^{-4} and 20 Mb/s at BERs lower than 7.0×10^{-3} at a link range of 0.53 m, achieving a 100% data rate improvement at a duty cycle of 0.5 and exceeding 100% when the duty cycle is less than 0.5 compared to baseline VLC. Notably, the completely linear dimming range covered 99.55% of the total dimming range, ensuring stable transmission even in darkness—a feature not supported by conventional VLC. The system also exhibited robustness across different terminal positions within a specific range. To further extend the communication range, three approaches can be considered to increase the received optical power: utilizing LDs with higher transmit power, employing LD arrays, and incorporating a lens at the transmitter to concentrate the light. Our future work will focus on dimming control experiments in the presence of user mobility.

REFERENCES

[1] Y. Hong and L.-K. Chen, "Toward user mobility for OFDM-based visible light communications," *Opt. Lett.*, vol. 41, no. 16, pp. 3763–3766, Aug. 2016.
[2] C. Lee et al., "26 Gbit/s LiFi system with laser-based white light transmitter," *J. Lightw. Technol.*, vol. 40, no. 5, pp. 1432–1439, Mar. 2022.
[3] H. Sugiyama, S. Haruyama, and M. Nakagawa, "Brightness control methods for illumination and visible-light communication systems," in *Proc. IEEE Int. Conf. Wireless Mobile Commun.*, 2007, pp. 78–83.
[4] F. Zafar, D. Karunatilaka, and R. Parthiban, "Dimming schemes for visible light communication: The state of research," *IEEE Wireless Commun.*, vol. 22, no. 2, pp. 29–35, Apr. 2015.
[5] H. Ji, T. Zhang, S. Qiao, and Z. Ghassemlooy, "Joint dimming control and optimal power allocation for THO-OFDM visible light communications," *IEEE Trans. Commun.*, vol. 69, no. 8, pp. 5352–5366, Aug. 2021.
[6] B. Li, X. Xue, S. Feng, and W. Xu, "Layered optical OFDM with adaptive bias for dimming compatible visible light communications," *J. Lightw. Technol.*, vol. 39, no. 11, pp. 3434–3444, Jun. 2021.
[7] T.-C. Bui, R. Singh, T. O'Farrell, and M. Biagi, "Optical energy-constrained slot-amplitude modulation for dimmable VLC: Suboptimal detection and performance evaluation," *IEEE Trans. Wireless Commun.*, vol. 20, no. 3, pp. 1582–1595, Mar. 2021.
[8] J. Guo, J. Zhang, G. Xin, and L. Li, "Constant transmission efficiency dimming control scheme for VLC systems," *Photonics*, vol. 8, no. 1, p. 7, Dec. 2020.

[9] G. Z. Abdelmessih, J. M. Alonso, and M. S. Perdigâo, "Hybrid series-parallel PWM dimming technique for integrated-converter-based HPF LED drivers," in *Proc. Int. Univ. Power Eng. Conf.*, 2016, pp. 1–6.

[10] I. E. Shaalan, E. M. Fadly, and M. H. Aly, "Enhanced ADO-OFDM-based adaptive digital dimming VLC system," *Opt. Lett.*, vol. 47, no. 9, pp. 2133–2136, May 2022.

[11] Y. Yang, C. Wang, C. Feng, C. Guo, J. Cheng, and Z. Zeng, "A generalized dimming control scheme for visible light communications," *IEEE Trans. Commun.*, vol. 69, no. 3, pp. 1845–1857, Mar. 2021.

[12] K. Lee and H. Park, "Modulations for visible light communications with dimming control," *IEEE Photon. Technol. Lett.*, vol. 23, no. 16, pp. 1136–1138, Aug. 2011.

[13] Y. Gu, N. Narendran, T. Dong, and H. Wu, "Spectral and luminous efficacy change of high-power LEDs under different dimming methods," in *Proc. 6th Int. Conf. Solid State Lighting*, 2006, pp. 78–84.

[14] J.-H. Choi, E.-B. Cho, and T.-G. Kang, "Pulse width modulation based signal format for visible light communications," in *Proc. Optoelectron. Commun. Conf. Tech. Dig.*, 2010, pp. 276–277.

[15] G. Ntogari, T. Kamalakis, J. Walewski, and T. Sphicopoulos, "Combining illumination dimming based on pulse-width modulation with visible-light communications based on discrete multitone," *J. Opt. Commun. Netw.*, vol. 3, no. 1, pp. 56–65, Jan. 2011.

[16] Z. Wang, W.-D. Zhong, C. Yu, J. Chen, C. P. S. Francois, and W. Chen, "Performance of dimming control scheme in visible light communication system," *Opt. Exp.*, vol. 20, no. 17, pp. 18861–18868, Aug. 2012.

[17] X. You, J. Chen, H. Zheng, and C. Yu, "Efficient data transmission using MPPM dimming control in indoor visible light communication," *IEEE Photon. J.*, vol. 7, no. 4, Aug. 2015, Art. no. 7902512.

[18] H. Elgala and T. D. C. Little, "Reverse polarity optical-OFDM (RPO-OFDM): Dimming compatible OFDM for gigabit VLC links," *Opt. Exp.*, vol. 21, no. 20, pp. 24288–24299, Oct. 2013.

[19] X. You, J. Chen, and C. Yu, "Efficient indoor data transmission with full dimming control in hybrid visible light/infrared communication systems," *IEEE Access*, vol. 6, pp. 77675–77684, 2018.

[20] E. Cho et al., "NRZ-OOK signaling with LED dimming for visible light communication link," in *Proc. IEEE Eur. Conf. Netw. Opt. Commun.*, 2011, pp. 32–35.

[21] H. Huang et al., "Experimental demonstration of optical camera communications supporting dimming control," in *Proc. IEEE Opto-Electron. Commun. Conf.*, 2023, pp. 1–4.

[22] D. Chen, J. Wang, J. Jin, H. Lu, and L. Feng, "A CDMA system implementation with dimming control for visible light communication," *Opt. Commun.*, vol. 412, pp. 172–177, Apr. 2018.

[23] H. Wu, Q. Wang, J. Xiong, and M. Zuniga, "SmartVLC: Co-designing smart lighting and communication for visible light networks," *IEEE Trans. Mobile Comput.*, vol. 19, no. 8, pp. 1956–1970, Aug. 2020.

[24] J. L. Henao-Rios, D. Marquez-Viloria, and N. Guerrero-González, "Real time implementation of a hybrid differential Manchester-PWM encoding for constant data rate under variable brightness in VLC systems," in *Proc. IEEE Colombian Conf. Commun. Comput.*, 2020, pp. 1–5.

[25] S. Das, B. Jana, and S. K. Mandal, "Implementation of dimming controlled visible light communication using Raspberry Pi," *Opt. Quantum Electron.*, vol. 53, pp. 1–19, Nov. 2021.

[26] M. A. S. Sejan, R. P. Naik, B. G. Lee, and W.-Y. Chung, "A bandwidth efficient hybrid multilevel pulse width modulation for visible light communication system: Experimental and theoretical evaluation," *IEEE Open J. Commun. Soc.*, vol. 3, pp. 1991–2004, 2022.

[27] X. You, J. Chen, Y. Zhong, S. Chen, and C. Yu, "Efficient dimming control with time domain hybrid modulation in indoor hybrid visible light/infrared communication systems," in *Proc. IEEE Opto Electron. Commun. Conf. Int. Conf. Photon. Switching Comput.*, 2019, pp. 1–3.

[28] J. R. Barry, *Wireless Infrared Communications*. Boston, MA, USA: Kluwer Academic, 1994.

[29] T. Komine and M. Nakagawa, "Fundamental analysis for visible-light communication system using LED lights," *IEEE Trans. Consum. Electron.*, vol. 50, no. 1, pp. 100–107, Feb. 2004.

[30] X. You, J. Chen, and C. Yu, "Performance of location-based equalization for OFDM indoor visible light communications," *IEEE Trans. Cogn. Commun. Netw.*, vol. 5, no. 4, pp. 1229–1243, Dec. 2019.

[31] F. Chang, K. Onohara, and T. Mizuochi, "Forward error correction for 100 G transport networks," *IEEE Commun. Mag.*, vol. 48, no. 3, pp. S48–S55, Mar. 2010.

[32] L. M. Zhang and F. R. Kschischang, "Staircase codes with 6% to 33% overhead," *J. Lightw. Technol.*, vol. 32, no. 10, pp. 1999–2002, May 2014.

[33] Z. Ghassemlooy, L. N. Alves, S. Zvanovec, and M.-A. Khalighi, *Visible Light Communications: Theory and Applications*. Boca Raton, FL, USA: CRC Press, 2017.

[34] T. Wang, F. Yang, J. Song, and Z. Han, "Dimming techniques of visible light communications for human-centric illumination networks: State-of-the-art, challenges, and trends," *IEEE Wireless Commun.*, vol. 27, no. 4, pp. 88–95, Aug. 2020.